Biosensors and Bioelectronics 141 (2019) 111398

Contents lists available at ScienceDirect

Biosensors and Bioelectronics

journal homepage: www.elsevier.com/locate/bios

# Graphene nanosheets as an electric mediator for ultrafast sensing of urokinase plasminogen activator receptor-A biomarker of cancer

Akanksha Roberts[a], Prem Prakash Tripathi[b,c], Sonu Gandhi[a,*]

[a] DBT-National Institute of Animal Biotechnology, Hyderabad, 500032, Telangana, India
[b] CSIR-Indian Institute of Chemical Biology (CSIR-IICB), Kolkata, 700091, India
[c] IICB-Translational Research Unit of Excellence, Kolkata, 700091, India

ARTICLE INFO

*Keywords:*
Fluorine doped tin-oxide
Graphene nanosheets
Urokinase type plasminogen activator receptor
Immunosensor
Cancer

ABSTRACT

Fluorine doped tin oxide (FTO) electrochemical immunosensor has been developed for rapid detection of urokinase type plasminogen activator receptor (uPAR) - a biomarker for cancer. uPAR is a GPI-anchored cell membrane receptor that shows increased expression in many types of human cancers which include breast, prostate, colorectal, and non-small cell lung cancer. In this study, a novel ultrasensitive FTO graphene nanosheets based electrode was used as a working probe to analyze the interaction between urokinase plasminogen activator (uPA) and monoclonal uPAR antibody (Ab). Graphene nanosheets (GNS) exhibited high conductivity, thereby increasing the sensitivity of the immunochemical assay. GNS were coupled with uPAR-Ab via carbodiimide activation chemistry with 1-ethyl-3-(3-dimethylaminopropyl)carbodiimide (EDC)/N-hydroxysuccinimide (NHS) as a heterobifunctional crosslinker. The confirmation of immobilization events was done by biophysical methods such as UV–Vis spectroscopy, fourier transform infrared spectroscopy (FTIR), scanning electron microscopy (SEM), atomic force microscopy (AFM), differential pulse (DPV), and cyclic voltammetry (CV). The immobilization conditions were optimized in accordance with the best sensor response. Under optimum conditions, the proposed sensor displayed wide linear detection range (1 fM to 1 μM) with a detection limit of 4.8 fM in standard. The developed sensor was profitably engaged to detect uPA in spiked serum samples up to 9.2 pM. Furthermore, the developed uPAR immunosensor showed good reproducibility, repeatability, and storage stability (75% of initial activity observed up to 4 weeks). FTO/GNS/uPAR-Ab/uPA-Ag immunosensor displayed acceptable performance for detection of uPA and exhibited low detection limit with high reproducibility. The proposed immunosensor is 'easy to use', highly specific, and can be used as a quantitative tool making it a tenable alternate for the detection of uPAR in cancer patients.

## 1. Introduction

Cancer diagnosis is very critical for prognosis, and is one of the major causes of death worldwide (Almasi, 2011). For the clinical diagnosis of cancer, histological analysis is considered to be the gold standard that contributes to poor prognosis, due to limitations in screening late-stage tumors that may already be too late to treat (Chan et al., 2016). Early prognosis will help in improving the recurrence of low grade cancer as well as avoid unnecessary chemotherapy. Increased uPAR expression has been observed in many types of cancers such as breast, prostate, colorectal, non-small cell lung, and lung (Mizukami et al., 1995; Montuori, 2003, 2013; Pedersen et al., 2003; Tomitaka et al., 2015). Urokinase-type plasminogen activator receptor (uPAR) is a GPI-anchored membrane protein which plays an important role in proteolysis and degradation of extracellular matrix protein (Dos et al., 2014; Zhao et al., 2015a; 2015b; Mahmood et al., 2018). uPA is a serine protease that is secreted in its inactive form called pro-uPA which binds to uPAR. Binding of pro-uPA with uPAR leads to the extracellular proteolytic pathway and catalyses the cleavage of plasminogen into plasmin. The uPAR receptor, shed from the cell membrane by phospholipase, is known as soluble uPAR (suPAR) and can be detected in human urine and plasma samples (Lomholt et al., 2009, 2010). uPAR regulates urokinase-type plasminogen activator (uPA) and plasminogen activator inhibitor-1 (PAI-1) that have been reported as prognostic factors in breast cancer patients. The elevated level of uPAR leads to poor diagnosis at early stage of invasion and metastasis (Mazar, 2008). Therefore, examination of tissue levels of urokinase-type plasminogen activator receptor (uPAR) can act as a milestone in early diagnosis of breast cancer patients (Tripathi et al., 2018). However, histological analysis, MRI or ELISA is time consuming, costly, and requires trained

* Corresponding author.
*E-mail address:* sonugandhi@gmail.com (S. Gandhi).

https://doi.org/10.1016/j.bios.2019.111398
Received 24 April 2019; Received in revised form 27 May 2019; Accepted 31 May 2019
Available online 31 May 2019
0956-5663/ 

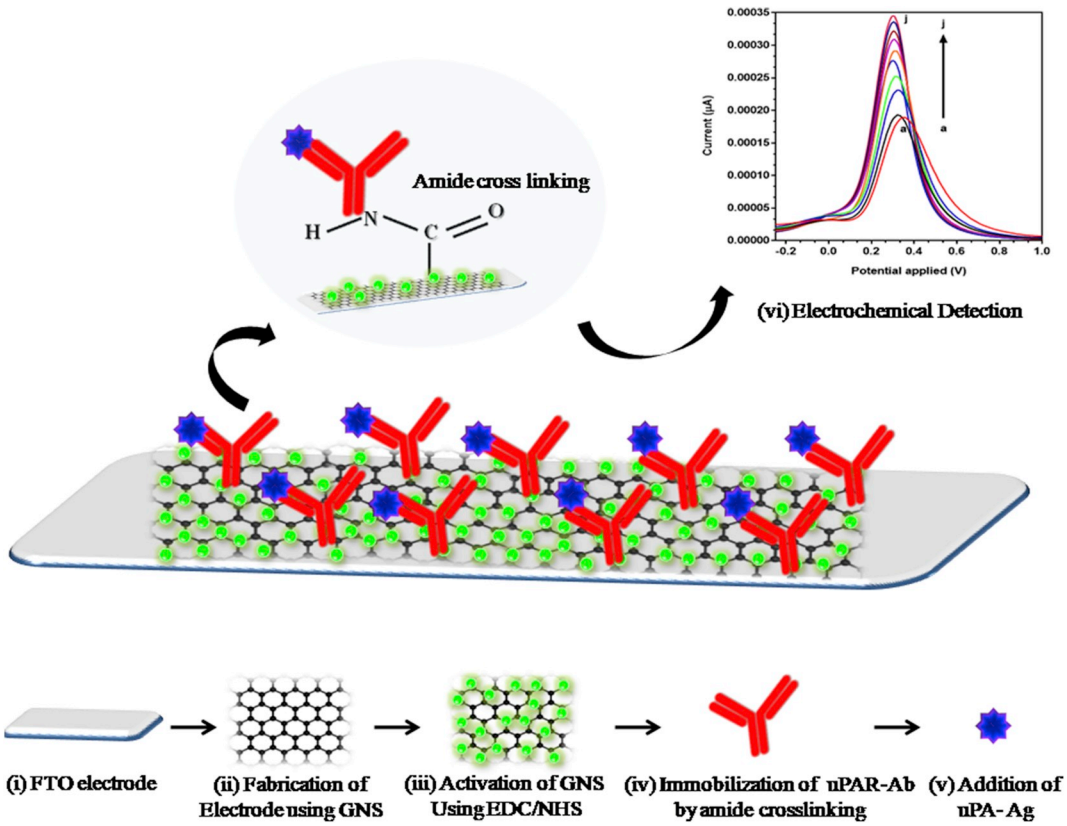


**Scheme 1.** Diagrammatic illustration of fabrication procedure. (i) bare FTO electrode as a platform for development of electrochemical immunosensor; (ii) Fabrication of FTO electrode by drop casting GNS; (iii) Activation of GNS using EDC and NHS; (iv) Immobilization of uPAR-Ab via amide crosslinking between activated GNS and Ab; (v) Addition of uPA-Ag (vi) Electrochemical Detection.

personnel (Lang et al., 2013; Fowler et al., 2014; Pedersen et al., 2003). Therefore, it is essential to develop a rapid, cost-effective and highly sensitive field applicable method for the detection of cancer. Electrochemical sensors have emerged in the clinical arena as the most preferred tool for early detection of cancer (Gandhi et al., 2016) because it provides efficiency with high specificity, along with ensuring competitive sensitiveness, cost effectiveness, robustness and versatility (Gandhi et al., 2018; Mishra et al., 2018; Islam et al., 2019a). Moreover, immunological interaction between a specific antigen and an antibody can be used as a detection method for the target analyte in a biological sample (Gandhi et al., 2008; Singh et al., 2018, Gandhi et al., 2015; Sharma et al., 2010). Coupling the advantages of immunological interactions and employing them for the development of electrochemical immunosensors can result in a highly specific and sensitive platform for cancer detection (Gandhi et al., 2016; Liu et al., 2018; Islam et al., 2019b). Most prominently used designs and configurations of the sensing elements utilized by research groups engaged in the development of electrochemical immunosensors include polymer-modified (Wijaya et al., 2009, 2010; Tey et al., 2010; Dervisevic et al., 2017), nanostructured (Pan et al., 2017; Pandey et al., 2017), screen-printed (Chan et al., 2016), and conventional (Liu et al., 2016) electrodes. Aptamer based electrochemical sensor has been developed for urokinase plasminogen activator receptor up to $10^{-12}$ - $10^{-9}$ M in a non-invasive manner for cancer detection (Jarczewska et al., 2015). MRI based contrast agent (GR-4Am-SA) includes a peptide that is susceptible for cleavage by uPA via chemical exchange saturation transfer (CEST) which provides a signal down to 9.5 ppm in *in-vivo* cancer detection (Sinharay et al., 2017). FTO (Fluorine-doped tin oxide) electrodes, being less expensive and more chemically stable, are preferred over ITO (Indium tin oxide) electrodes (Yu et al., 2016). Choosing a suitable nanomaterial is also of utmost importance and graphene nanosheets (GNS) have emerged as the most viable option in biosensing applications due to their ultrahigh surface-to-volume ratio and electrochemical properties (Fan and Shen, 2015; Krishnan et al., 2019).

The customarily utilized biomolecules, as the recognition element for sensors, include antibodies (Gandhi et al., 2008; Suri et al., 2008, 2009; Gandhi et al., 2009), nucleic acids (Souza e Silva et al., 2016), aptamers (Jarczewska et al., 2015) and peptides (Hwang et al., 2017). Antibodies have emerged as a novel biosensing tool for rapid detection of various analytes due to its specific immunological interaction, thus providing biosensors with high specificity and sensitivity for disease detection (Hyun et al., 2016).

The present study describes, for the first time, development of a novel and sensitive electrochemical immunosensor for the detection of uPAR that plays a pivotal role in cancer invasion and metastasis. The FTO electrode was developed due to its high electrical conductivity, stability under atmospheric conditions and high tolerance to physical abrasion which makes it an ideal platform for electrochemical biosensing application (Talan et al., 2018). Graphene nanosheets (GNS) were coupled with anti-uPAR antibody for amplification of the sensing signal. The conjugate (GNS/anti-uPAR-Ab) was characterized using various bioanalytical and electrochemical techniques viz UV–Vis spectroscopy, Dynamic Light Scattering (DLS), X-Ray Diffraction (XRD), Scanning Electron Microscopy (SEM), cyclic voltammetry (CV), and differential pulse voltammetry (DPV). FTO-GNS/anti-uPAR-Ab based electrochemical sensor was developed for uPAR detection and can be used for real sample analysis in cancer diagnostics.

## 2. Materials and methods

### 2.1. Reagents

FTO-electrode was purchased from Sigma (India). uPA antigen (uPA-Ag), monoclonal Anti-uPAR antibodies (anti-uPAR-Ab) and goat

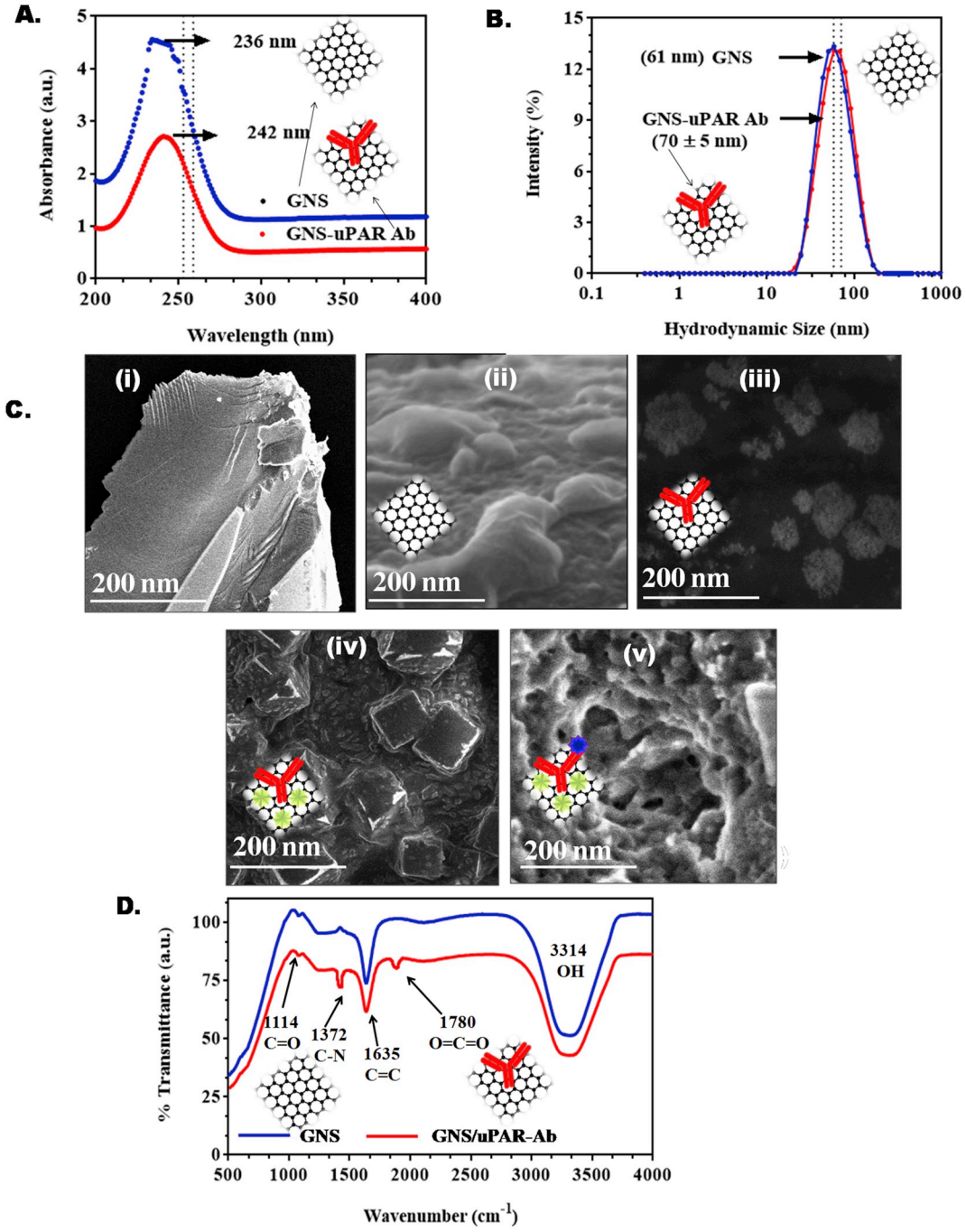


**Fig. 1.** Uv–Vis spectrum (A) at 236 nm displayed GNS synthesis. uPAR-Ab binding to GNS was affirmed by peak shift from 236 nm to 242 nm; (B) DLS spectra of GNS (61 nm) and GNS-uPAR-Ab (70 nm); (C) SEM morphology of GNS and uPAR-Ab showed the (i) bulk GNS, (ii) monolayered GNS, (iii) GNS-$COO^-$, (iv) GNS/uPAR-Ab was seen as a uniformly distributed globular structure (v) GNS/uPAR-Ab/Ag; (D) FT-IR spectra showed the presence of C≡N stretch at 1372 $cm^{-1}$ wavenumber confirmed the binding of antibody with GNS further.

serum were procured from Sigma, India. Reagents required for the preparation of buffers such as potassium ferricyanide ($K_3Fe(CN)_6$), potassium ferrocynaide ($K_4Fe(CN)_6.3H_2O$), sodium hydrogen phosphate ($Na_2HPO_4$), potassium dihydrogen phosphate ($KH_2PO_4$) and potassium chloride (KCl) were purchased from Sigma (India). Melamine, Sodium hydroxide (NaOH), glycerol, sulfuric acid ($H_2SO_4$) and ethanol ($CH_3CH_2OH$) were purchased from Sigma for GNS synthesis. Activation of GNS was done using 1-Ethyl-3-(3-dimethylaminopropyl)carbodiimide (EDC) and N-Hydroxysuccinimide (NHS) obtained from Sigma, India. Other reagents, chemicals and solvents used in the experimental study were of high purity and analytical grade. Double distilled water (DDW) was used for preparation of all solutions.

### 2.2. Apparatus

UV–Vis spectrophotometer (Systonic, India, S925) was utilized to obtain UV–Vis spectrum. Differential pulse voltammetry (DPV) and Cyclic voltammetry (CV) measurements were taken using PGSTAT Autolab-10, Eco Chemie, Netherlands operated by NOVA software. Sn-oxide electrode doped with fluorine (FTO, having working dimensions as 1 cm and 3 cm) was obtained from Merck, India. Three-electrode arrangement (comprising of auxiliary, working and reference electrodes) at ambient room temperature of 25 ± 1 °C was employed in performing the required set of experiments. DLS readings were taken through the Nicomp 380 ZLS from Particle sizing systems, Port Richey,

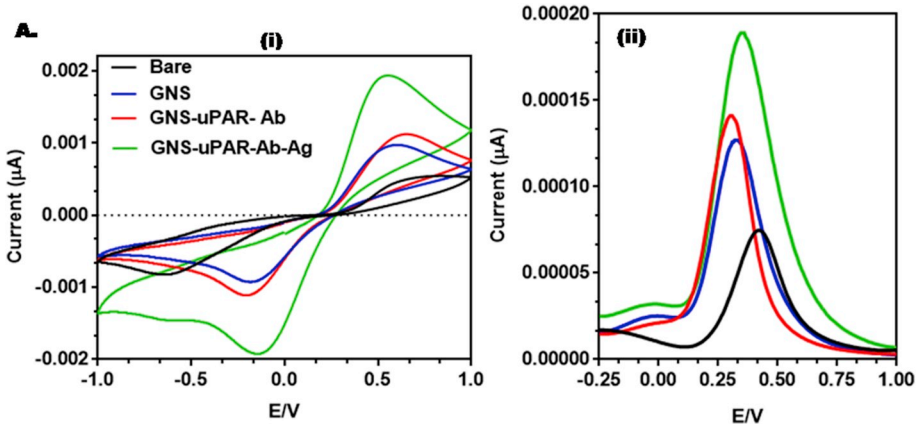


**Fig. 2.** Characterization of FTO electrode; (i) Cyclic voltammogram (CV) of FTO, FTO-GNS, FTO-GNS/uPAR-Ab along with FTO-GNS/uPAR-Ab/uPA-Ag electrode in the scanned potential range of −0.001 kV to 0.001 kV in 0.1 M KCl, having 0.005 M $K_4Fe(CN)_6.H_2O$ and 0.005 mM $K_3Fe(CN)_6$ with buffer pH 7, at scan rate 100 mV/s (ii) Differential pulse voltammogram (DPV) of FTO, FTO-GNS and FTO-GNS/uPAR-Ab, and FTO-GNS/uPAR-Ab/uPA-Ag electrode in scanned potential range 0–0.0015 kV in 100 mM potassium chloride (KCl) having 0.005 M $K_4Fe(CN)_6.H_2O$ and 0.005 M $K_3Fe(CN)_6$ buffer pH 7.0, at 100 mV/s as the scan rate.

FL, USA operated via definite source of green monochromatic excitation at 532nm/0.05 W. For performing SEM analysis, JEOL USA-JEN 2010 was utilized, with 200 kV as the accelerating voltage.

### 2.3. rGO synthesis and its labeling with uPAR-Ab

Reduced graphene oxide (rGO) was synthesized by a modified Hummer's method (Hummers and Richard, 1958). For the synthesis of rGO, graphite powder (1 g) was mixed with 25 mL of concentrated $H_2SO_4$. The mixture was cooled and 3 g of $KMnO_4$ added. 200 mL of DI $H_2O$ was added while stirring that led to the formation of a black coloured mixture. The mixture was then washed with 5% HCl and dried under ambient conditions for GO synthesis. 20 mg of GO was then sonicated and autoclaved in a PTFE lined stainless steel chamber for 4 h followed by washing with acetone and water. The resulting rGO was allowed to dry at RT overnight. The images of SEM exposed that carbon spheres were absent in the product, comprising merely of thin sheets. GNS was then labeled with uPAR-Ab by using carbodiimide chemistry. In detail, EDC (75 μm) and NHS (75 μm) was used at equimolar ratio in 1x PBS, pH 7.4 and added dropwise to GNS (1 mg). The reaction mix was allowed to incubate at RT for 1 h followed by fabrication on the surface of electrode by addition of different ratios of uPAR-Ab (0.25, 0.5, 1.0, 1.5 μg) to obtain best optimal concentration followed by incubation at 4 °C.

### 2.4. Characterization of GNS and GNS/uPAR-Ab

UV–Vis spectrophotometer was used for observing the synthesis of GNS. A confined scale from 20 nm to 8 nm with a step of 0.1 nm was observed as the absorption spectrum, with a scan rate up to 20 nm/s. The hydrodynamic diameter was calculated using DLS technique with frequency at 200 kHz, angle of scattering at 90 °C, and measured media temperature at 24 ± 2 °C. Stokes–Einstein equation as described previously was applied to calculate the hydrodynamic diameter of GNS and GNS/uPAR-Ab. Water was considered as the continuous phase (water viscosity = 911000–852000 Pa/s). Morphological analysis was determined by SEM. Deposited specimen present over SEM grid, coated with carbon, was air dried for a few minutes before analysis by putting a drop of solution. FT-IR studies were done for functional group analysis using IRTracer-100 FTIR Spectrometer, Shimadzu. Comparative analysis was done for all characterization methods for GNS and GNS/uPAR-Ab.

### 2.5. FTO-GNS/uPAR-Ab electrode fabrication and characterization

The FTO (3 cm × 1 cm) electrode was made up of glass and coated with fluorine doped tin oxide while reference electrode was Ag/AgCl. GNS was activated using carbodiimide chemistry (EDC-NHS) (75 μm each) for 2 h, followed by fabrication of GNS (200 μL) on FTO electrode at room temperature (RT). uPAR-Ab (0.25, 0.5, 1.0, 1.5 μg) was immobilized for 24 h at 4 °C.

Cyclic voltammetry (CV) was employed for analysis of the electrochemical properties of FTO-GNS/uPAR-Ab electrode. This was done by broadening the value of potential starting from −0.001 kV to 0.001 kV in potassium ferricynanide/potassium ferrocyanide (1:1) solution having 100 mM KCl (Talan et al., 2018). In order to obtain maximum sensing signal, optimization of various factors including response time, pH, temperature, antibody concentration, and scan rate was done. Various concentration ranges from 1 fM to 1 μM (in 1x PBS, pH 7.4) of uPA-Ag were employed for electrochemical characterization.

### 2.6. Relevance of modeled immunosensor in spiked serum samples-

Developed immunosensor was assessed for its degree of sensitivity and extent of specificity in spiked samples of cancer antigen (uPA-Ag). Different concentrations of antigen (1 fM to 1 μM) were spiked in goat serum sample. The electrochemical response was calculated using potassium ferricynanide/potassium ferrocyanide (1:1) solution having 100 mM KCl, to determine the presence of uPA-Ag. Cross reactivity studies were also carried out at similar concentrations in order to check the specificity using progesterone (prg), HIV (HIV) and anti-cardiac troponin (cTn1) antigen.

## 3. Results and discussion

### 3.1. Outline and principle of the designed FTO immunosensor

Scheme 1 elucidates the fabrication theory of the designed FTO based immunosensor integrated with GNS and uPAR-Ab. FTO surface immobilized with GNS serves as a link for amplification of the signal due to its elevated electrical conductivity. Besides this, GNS also serves as a suitable platform for uPAR-Ab immobilization via covalent or electrostatic interactions. In order to obtain a uniform layer on the FTO electrode, physiosorption of GNS was done so as to attain high electrical conductivity. Immobilization of uPAR-Ab on GNS fabricated FTO electrode was done using carbodiimide chemistry. Addition of uPAR-Ab led to changes in the electrical current, which thereby confirmed the use of immunosensor for the detection of uPA. Effect of different concentrations of uPAR-Ab provided linear response with respect to change in current. As the concentration increased, current response increased, and after a certain point, the current response decreased. The major phenomenon that lies behind this is the orientation and polarity of the protein molecules that plays a crucial role in electron transfer from the electrode surface. The developed immunosensor possesses beneficial features of GNS, FTO electrode and highly specific immunological interaction between uPAR-Ab and uPA-Ag, producing quick and effective response with very low limit of detection (LOD).

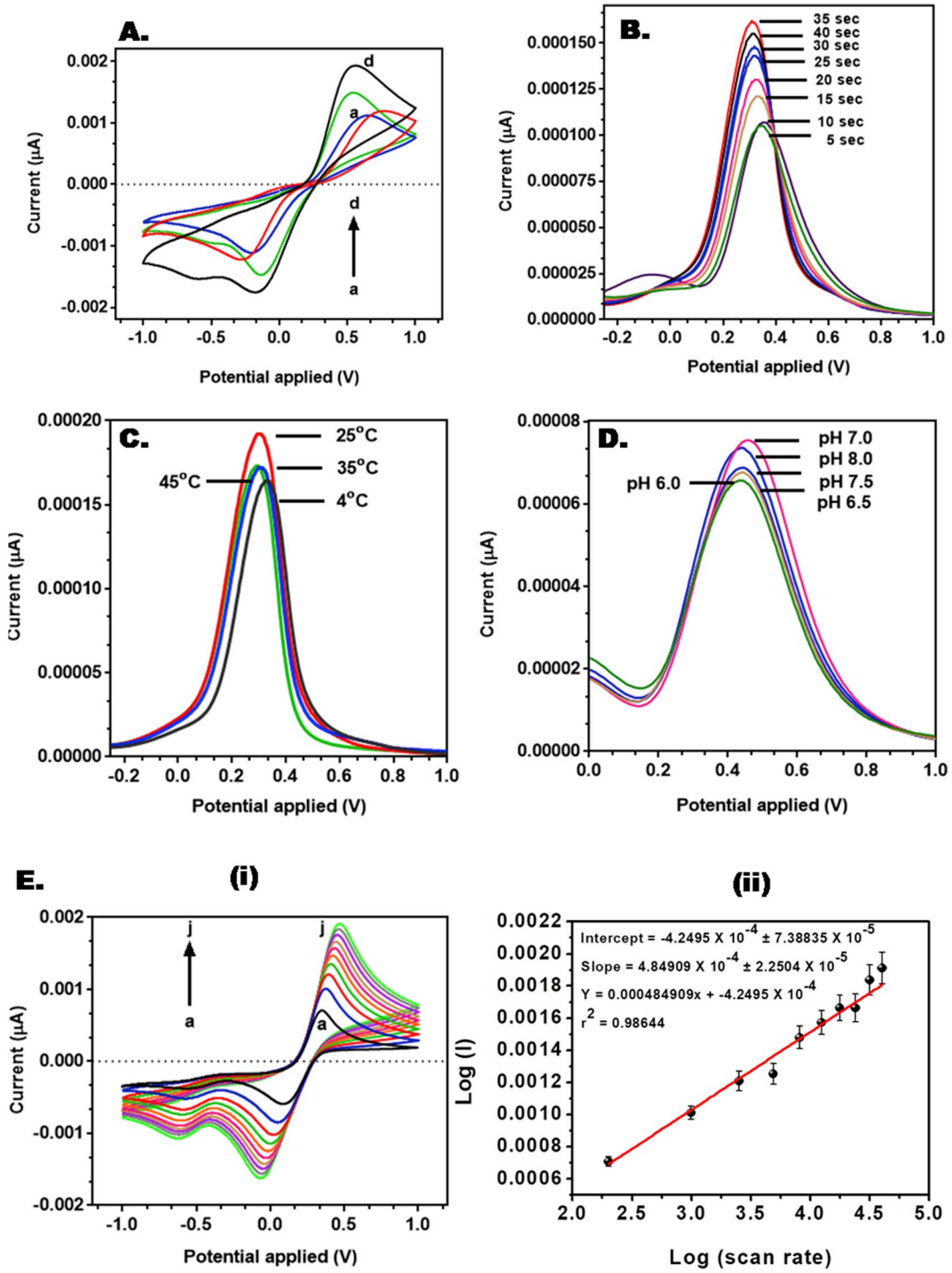


**Fig. 3.** CV measurements for FTO-GNS/uPAR-Ab (A) at various concentrations of uPAR-Ab viz., (a) 0.25 (b) 0.50 (c) 1.0, and (d) 1.5 μg (with 0–1.5 V as the scanning potential range); (B) at various response time in the range 5–40 s in similar conditions as in Fig. 2A; (C) at different temperatures 4, RT, 35 and at 45 °C; (D) at different pH range 6.0–8.0; (E) CV measurements for (E-i) Optimization of different scan rates from 0.01 to 0.1 V/s; (E-ii) Calibration curve involving log of scan rates. 0.1 M KCl with 0.005 M $K_4Fe(CN)_6.3H_2O$ and 0.005 M $K_3Fe(CN)_6$ pH 7.0 were used as buffer for all the optimization studies.

### *3.2. Characterization of FTO based immunosensor*

Uv–Vis spectra were recorded in the range of 200–800 nm for GNS and GNS/uPAR-Ab (Fig. 1 A). The peak of GNS was observed at 236 nm while binding of GNS and uPAR-Ab was assured by a red shift of 6 nm from 236 to 242 nm. The widening of the peak was also observed that might indicate the successful labelling reaction of GNS with antibody. The binding event was further validated by change in hydrodynamic diameter from 61 nm (GNS) to 70 nm (GNS/uPAR-Ab) as shown in Fig. 1B. It was seen that GNS were present in monodispersed state with narrow diameter distribution having an average diameter of 65 nm. SEM was done for morphological studies at each step of fabrication, bulk to GNS synthesis, GNS functionalization (GNS-$COO^-$) to antibody immobilization (GNS/uPAR-Ab), and further antigen binding (GNS/uPAR-Ab/uPA-Ag) as depicted in Fig. 1C (i-v) respectively. Fig. C-i appeared as white crystalline rock that comprises of bulk GNS while after GNS synthesis, it looks like a thin sheet of carbon (Fig. C-ii). The uPAR-Ab was immobilized on to activated graphene, as shown in

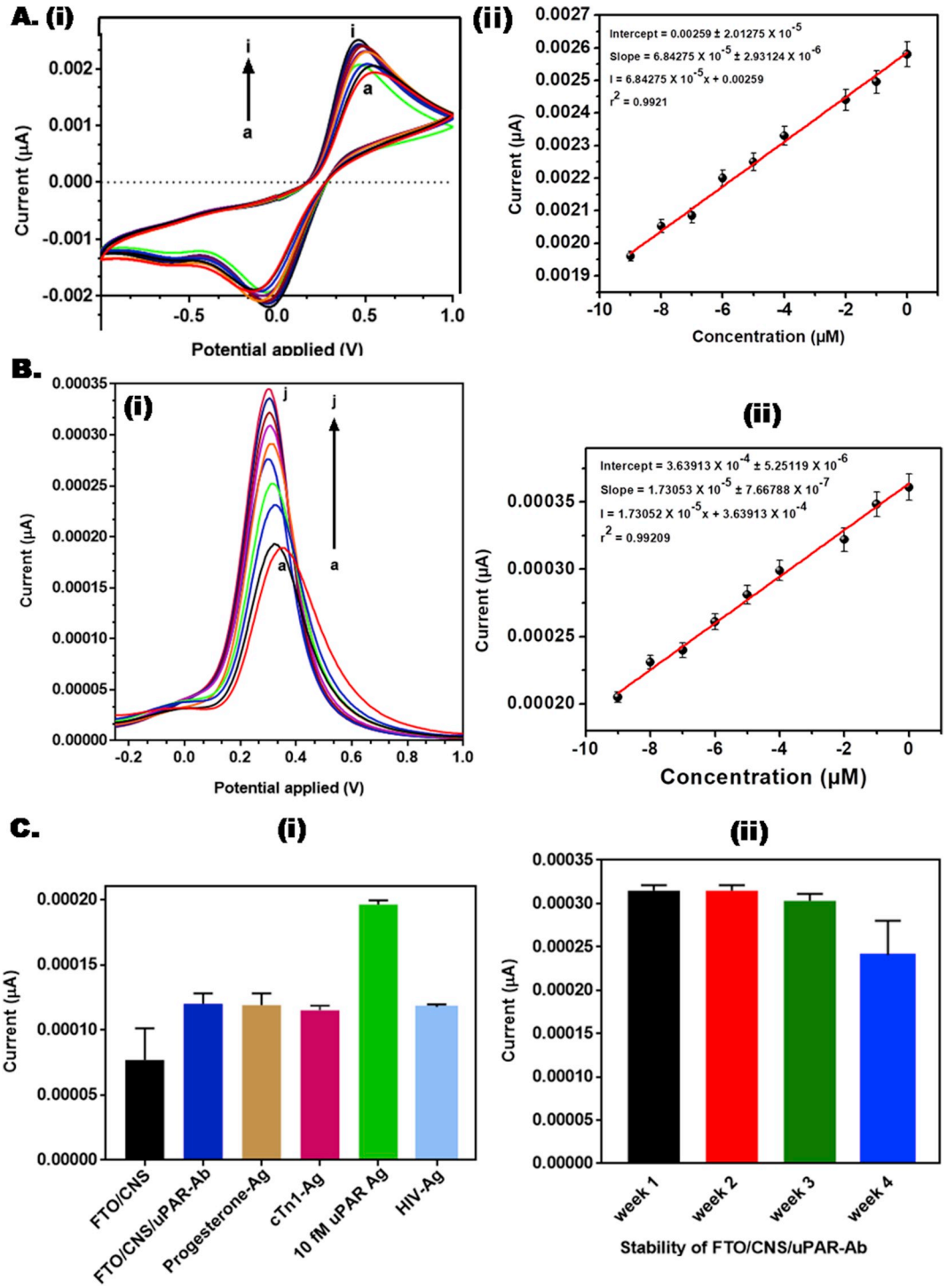


**Fig. 4.** (A-i) CV at various uPA-Ag concentrations (i) 1 μM (ii) 100 nM (iii) 10 nM (iv) 1 nM (v) 100 pM (vi) 10pM (vii) 1 pM (viii) 100 fM (ix) 10 fM (x) 1 fM in scanning potential range 0 V–1.5 V. (B-i) DPV of the same as given in figure A–I; (A-ii &B-ii) Standard calibration plot corresponding to A-I & B-i; (C-i) Cross reactivity studies in spiked samples (progesterone (prg), HIV, and cardiac troponin marker (cTn1)); (C-ii) Stability studies of FTO-GNS/uPAR-Ab electrode on $0^{th}$ day, 7th day, 14th day and 21st day. uPA-Ag was used at 10.0 fM in scanning potential range similar in Fig. 2.

Fig. 1C (iii) as uniform, white globular structures on GNS plane. The graphene bound uPAR-Ab were treated with 5% BSA to block unbound sites and can be seen in the form of crystal like structures in Fig. 1C (iv). Furthermore, uPA-Ag was added to confirm the binding in Fig. 1C (v). FT-IR spectra (Fig. 1 D) was obtained for similar samples before carrying out electrochemical analysis that proved the presence of C≡N stretch together with O–H, O═C═O, C═C, C═O bonds at 1372, 3314, 1780, 1635, and 1114 $cm^{-1}$ wave number. C≡N stretch provides the gateway for bonding of amino group of uPAR-Ab to carboxylic group of activated GNS. The obtained series of results clearly signified that the GNS were effectively labeled with uPAR-Ab using carbodiimide chemistry, and thus, can be employed further for the electrochemical optimization in fabrication of FTO electrode.

**Table 1**
Comparison of our method with various approaches for urokinase detection in cancer patients-.

| Methodology | Limit of detection (LOD) | Linear range | Type of study | References |
|---|---|---|---|---|
| MRI | 5ppM | – | In-vivo | Sinharay et al. (2017). |
| ELISA | 1.78 ng/mG | 0–22.76 ng/mG | In-vivo | Taubert et al. (2010) |
| Photoelectrochemical | 33 fg/mL | 1 μg/mL – 0.1 pg/mL | _ | Liu et al. (2018) |
| ELISA | < 3 pmol/L | 1–10000 nmol/L | _ | Piironen et al., 2004 |
| FTO-GNS-uPAR-Ab electrode | 4.8 fM | 1 fM to 1 μM | 35 s | This paper |

### 3.3. Electrochemical characterization of immunosensor

Electrochemical characterization was done for bare FTO, GNS and GNS/uPAR-Ab modified electrodes and ferro/ferricyanide was used as a redox probe in cyclic voltammograms (CV) (Fig. 2). When compared to the electrode modified with GNS, bare electrode reflected static response to the redox probe (solid curvature) due to high conductivity of GNS that is responsible for accelerating the transfer rate of electrons (Talan et al., 2018). The added benefits of high surface area of GNS may have been ascribed due to the increased electron transfer permeability from ferrocyanide. The exact mechanism for this is still unknown. Bioconjugation of uPAR-Ab followed by uPA-Ag generates increased sensing signal as compared to GNS modified FTO which may be attributed to the insulating behavior of uPAR-Ab and uPA-Ag that causes enhanced electron transport. The obtained CV (Fig. 2A(i)) was further validated by differential pulse voltammogram (DPV) (Fig. 2A(ii)) and both results were corresponding to each other.

### 3.4. Optimization of variable parameters of FTO-GNS/uPAR-Ab electrode

The concentrations of uPAR-Ab (0.25–1.5 μg) were optimized at 1.0 μg in order to attain maximum analytical performance by electrode (Fig. 3A). Response time was calculated from 5 s to 35 s, based on the evaluation of sufficient immunological interaction between uPAR-Ab and uPA-Ag. The increase in maximum peak current response was observed at 35 s with a gradual drop in current response after 40 s. Thus, the optimum response time was kept at 35 s for specific antigen-antibody interaction (Fig. 3B). In order to determine the effect of temperature on the electrode performance generated due to current, electrode was kept at different temperatures (4, 25 room temperature (RT), 35, 45 °C). At RT, the current response was amplified whereas a decrease in current response was observed at 35 and 45 °C. Therefore, the subsequent experimental studies were done at optimum temperature (25 °C) (Fig. 3C). Also, the optimization of the fabricated FTO-GNS/uPAR-Ab electrode was done from pH 6.0 to 8.0, as depicted in Fig. 3D. The highest current was observed at pH 7 and thus, was used further in binding studies for analyzing standard and spiked samples. The scan rates (10–100 mV/s) were measured for best electrode performance with FTO-GNS/uPAR-Ab electrode and CV measurements were recorded. Sharp anode and cathode peaks were noticed for anti-uPAR-Ab that clearly defines the stable nature of the fabricated electrode (Fig. 3E(i)). Increase in scan rate is directly proportional to the degree of the peak current. The calibration curve was plotted and values corresponding to the slope, intercept and coefficient of correlation have been mentioned in the equations below. At 100 mV/s, peak current dependency (I) on scan rate (square root) is shown by the following expression: Intercept = $-4.2495 \times 10^{-4} \pm 7.38835 \times 10^{-5}$; Slope = $4.84909 \times 10^{-4} \pm 2.2504 \times 10^{-5}$; $Y = 0.000484909x + -4.2495 \times 10^{-4}$; $r^2 = 0.98644$.

### 3.5. Analytical performance of FTO-GNS/uPAR-Ab electrode

Cyclic voltammetry (CV) and Differential pulse voltammogram (DPV) were recorded to analyze the electrode performance at optimal state (Fig. 4A(i) &B(i)). A strong linear association was observed between current (I) and logarithm of uPA-Ag concentrations in the range 1 fM to 1 μM. With increasing concentrations of anti-uPAR-Ab, there was subsequent increase in the peak current. Fig. 4A(ii) & B(ii) represents the regression equation for CV and DPV. The intercept for CV was $0.00259 \pm 2.01275 \times 10^{-5}$ and slope was $6.84275 \times 10^{-5} \pm 2.01275 \times 10^{-5}$ with equation $I = 6.84275 \times 10^{-5}x + 0.00259$ and $r^2$ value of 0.9921. For DPV, the intercept value was recorded as $3.63913 \times 10^{-4} \pm 5.25119 \times 10^{-6}$ and slope was $1.73053 \times 10^{-5} \pm 7.66788 \times 10^{-7}$, thus the equation was $I = 1.73052 \times 10^{-5}x + 3.63913 \times 10^{-4}$ with $r^2$ value = 0.99209, where I corresponds to the current and c signifies uPA-Ag concentration. The detection range as well as the limit of detection (LOD) in standard samples was observed as 1 fM to 1 μM and 4.8 fM respectively in standard samples. Due to high conductance of GNS, a high sensitivity with improved signal amplification was reflected in the developed FTO-GNS/uPAR-Ab based immunosensor.

### 3.6. Cross-reactivity studies with FTO-GNS-uPAR-Ab electrode

FTO-GNS/uPAR-Ab electrode based cross reactivity studies were conducted using progesterone (prg), HIV (HIV), and anti-cardiac troponin (cTn1) antigen in linear concentration range of 1 fM to 1 μM. Insignificant change in peak current (Fig. 4C–i) was observed. Experiment dealing with binding activity was also performed under similar conditions for FTO-GNS/uPAR-Ab and uPA-Ag. A considerable increase in current response was noticed due to the addition of uPA-Ag with LOD up to 9.2 pM in spiked serum samples. Table 1 represents a relative outlook of detection systems developed till date for uPAR. Besides regeneration, stability factors were also examined for FTO-GNS/uPAR-Ab fabricated electrode, revealing remarkable results. In order to fulfill the same, the fabrication of a set of five electrodes done in order to study the stability response with time, showed no change in electric current (Fig. 4C–ii). Repeatability of the designed immunosensor was consistent on various days viz 1st week (7th day), 2nd week (14th day) and 3rd week (21st day) of its fabrication. Response for DPV was examined at 100 fM of uPA-Ag. The fabricated electrode component was kept at 4 °C up to 21 days. There was a slight drop in peak current post 21 days, thus reconfirming high stability of the FTO-GNS/uPAR-Ab electrode. The results obtained in relation to the FTO-GNS/uPAR-Ab electrode were promising which makes the developed sensing platform applicable for the detection of various other diseases.

## 4. Conclusion

Conclusively, we successfully developed a new ultrasensitive FTO-GNS/uPAR-Ab based electrochemical biosensor for uPA detection in cancer with a rapid response time of 35 s. Use of smart nanomaterial for fabrication of FTO electrode, such as graphene nanosheets (GNS), increases the sensitivity of the sensor due to fast conduction of electrons. The range of linearity of the proposed immunosensor was 1 fM to 1 μM with a low limit of detection up to 9.2 pM. The developed sensor not only overcomes the challenges associated with response of the sensor but also solves the sensitivity issues. The sensor reported in the present study is highly efficient for early detection of cancer in patients and could be applicable on-site after suitable fabrication. It is assumed that further improvement could be possible by improving the device

characteristics on the limit of detection (LOD) lower than pM concentration. In addition, advancement in future device optimization techniques, is believed to be additional promising approach for consideration. The present work can also be expanded to successfully detect various other diseases with inexpensive and beneficial options.

## Acknowledgement

SG wrote and conceptualize the manuscript. AR helped in the correction of the manuscript. PPT helped in the discussion during writing the manuscript. The research endowment, DST/ECR/2016/000075 secured from Department of Science and Technology (DST), New Delhi, and grant number BT/PR18069/BIC/101/574/2016 from Department of Biotechnology (DBT-Biocare), New Delhi, India is highly acknowledged with regard to their immense support to take forth the research task.

## References

Almasi, C.E., 2011. Lung Cancer 74, 510–515.
Chan, K.F., Lim, H.N., Shams, N., Jayabal, S., Pandikumar, A., Huang, N.M., 2016. Mater. Sci. Eng. C Mater. Biol. Appl. 58, 666–674.
Dervisevic, M., Dervisevic, E., Senel, M., Cevik, E., Yildiz, H.B., Camurlu, P., 2017. Enzym. Microb. Technol. 102, 53–59.
Dos, A.P.B., da Luz, F.A., de Faria, P.R., Oliveira, A.P., de Araujo, R.A., Silva, M.J., 2014. J. Cancer 5, 559–571.
Fan, H., Shen, W., 2015. Chem. Sus. Chem. 8, 2004–2027.
Fowler, C.B., Man, Y.G., Mason, J.T., 2014. J. Cancer 5, 115–124.
Gandhi, S., Arami, H., Krishnan, K.M., 2016. Nano Lett. 16, 3668–3674.
Gandhi, S., Banga, I., Maurya, P.K., Eremin, S.A., 2018. RSC Adv. 8, 1511–1518.
Gandhi, S., Sharma, P., Capalash, N., Verma, R.S., Suri, C.R., 2008. Anal. Bioanal. Chem. 392, 215–222.
Gandhi, S., Capalash, N., Sharma, P., Suri, C.R., 2009. Biosens. Bioelectron. 25, 502–505.
Gandhi, S., Sharma, P., Capalash, N., Suri, C.R., 2015. Bioimpacts 5, 207–213.
Hummers, W.S.O., Richard, E., 1958. J. Am. Chem. Soc. 80 1339-1339.
Hwang, H.J., Ryu, M.Y., Park, C.Y., Ahn, J., Park, H.G., Choi, C., Ha, S.D., Park, T.J., Park, J.P., 2017. Biosens. Bioelectron. 87, 164–170.
Hyun, K., Ueno, T., Li, O.L., Saito, N., 2016. RSC Adv. 6, 6990–6996.
Islam, S., Shukla, S., Bajpai, V.K., Han, Young-Kyu, Huh, Y.S., Ghosh, A., Gandhi, S., 2019a. Biosens. Bioelectron. 126, 792–799.
Islam, S., Shukla, S., Bajpai, V.K., Han, Young-Kyu, Huh, Y.S., Ghosh, A., Gandhi, S., 2019b. Sci. Rep. 9, 276–282.
Jarczewska, M., Kekdy-Nagy, L., Nielsena, J.S., Campos, R., Kjemsa, J., Malinowska, E., Ferapontov, E.E., 2015. Analyst 140, 3794–3802.
Krishnan, S.K., Singh, E., Singh, P., Meyyappan, M., Nalwa, H.S., 2019. RSC Adv. 9, 8778–8881.
Lang, D.S., Heilenkötter, U., Schumm, W., Behrens, O., Simon, R., Vollmer, E., Goldmann, T., 2013. Breast 22, 736–743.
Liu, Xing-Pei, Chen, Jing-Shuai, Mao, Chang-jie, Niu, He-Lin, Song, Ji-Ming, Jin, Bao-Kang, 2018. Anal. Chim. Acta 1025, 99–107.
Liu, X., Marrakchi, M., Xu, D., Dong, H., Andreescu, S., 2016. Biosens. Bioelectron. 80, 9–16.
Lomholt, A.F., Høyer-Hansen, G., Nielsen, H.J., Christensen, I.J., 2009. Br. J. Canc. 101, 992–997.
Lomholt, A.F., Christensen, I.J., Høyer-Hansen, G., Nielsen, H.J., 2010. Acta Oncol. 49, 805–811.
Mahmood, N., Mihalcioiu, C., Rabbani, S.A., 2018. Front. Oncol. 8, 1–21.
Mazar, A.P., 2008. Clin. Cancer Res. 14, 5649–5655.
Mishra, P., Banga, I., Tyagi, R., Munjal, T., Goel, A., Capalash, N., Sharma, P., Suri, C.R., Gandhi, S., 2018. RSC Adv. 8, 23163–23170.
Mizukami, I.F., Faulkner, N.E., Gyetko, M.R., Sitrin, R.G., Todd, R.F., 1995. Blood 86, 203–211.
Montuori, N., 2013. Thromb. Haemostasis 109, 309–318.
Montuori, N., 2003. Int. J. Cancer 105, 353–360.
Pan, L.H., Kuo, S.H., Lin, T.Y., Lin, C.W., Fang, P.Y., Yang, H.W., 2017. Biosens. Bioelectron. 89, 598–605.
Pandey, A., Gurbuz, Y., Ozguz, V., Niazi, J.H., Qureshi, A., 2017. Biosens. Bioelectron. 91, 225–231.
Pedersen, N.H., Mouridsen, T., Tenney, D.Y., Brünner, N., 2003. Eur. J. Cancer 39, 899–908.
Piironen, T., Laursen, B., Pass, J., List, K., Gårdsvoll, H., Ploug, M., Danø, K., Høyer-Hansen, G., 2004. Clin. Chem. 50, 2059–2068.
Sharma, P., Gandhi, S., Suri, C.R., 2010. Anal. Chim. Acta. 676, 87–92.
Sinharay, S., Howison, C.M., Baker, A.F., Pagel, M.D., 2017. NMR Biomed. 30, 1–16.
Singh, S., Mishra, P., Banga, I., Parmar, A.S., Tripathi, P.P., Gandhi, S., 2018. Bioimpacts 8, 57–62.
Souza e Silva, T.D., Castro, A.C.H., Rodovalho, V.R., Madurro, J.M., Brito-Madurro, A.G., 2016. J. Solid State Electrochem. 20, 2411–2418.
Suri, C.R., Kaur, J., Gandhi, S., Shekhawat, G., 2008. J. Nanotechnol. 19, 235502.
Suri, C.R., Boro, R., Nangia, Y., Gandhi, S., Wangoo, N., Sharma, P., Shekhawat, G.S., 2009. Trends Anal. Chem. 28, 29–31.
Talan, A., Mishra, A., Eremin, S.A., Narang, J., Kumar, A., Gandhi, S., 2018. Biosens. Bioelectron. 105, 14–21.
Taubert, H., Würl, P., Greither, T., Kappler, M., Bache, M., Lautenschläger, C., Füssel, S., Meye, A., Eckert, A.W., Holzhausen, H.-J., Magdolen, V., Kotzsch, M., 2010. Br. J. Canc. 102, 731–737.
Tey, J.N., Gandhi, S., Wijaya, I.P.M., Palaniappan, A., Wei, J., Rodriguez, I., Suri, C.R., Mhaisalkar, S.G., 2010. Small 6, 993–998.
Tomitaka, A., Arami, H., Gandhi, S., Krishnan, K.M., 2015. Nanoscale 7, 16890–16898.
Tripathi, P.P., Arami, H., Banga, I., Gupta, J., Gandhi, S., 2018. Oncotarget 9, 37252–37267.
Wijaya, I.P.M., Gandhi, S., Tey, J.N., Wangoo, N., Shekhawat, G., Suri, C.R., Rodriguez, I., Mhaisalkar, S.G., 2009. Appl. Phys. Lett. 95, 073704.
Wijaya, I.P.M., Tey, J.N., Gandhi, S., Boro, R., Rodriguez, I., Mhaisalkar, S.G., Suri, C.R., Palaniappan, A., Hau, G.W., 2010. Lab Chip 10, 634–638.
Yu, S., Li, L., Lyu, X., Zhang, W., 2016. Sci. Rep. 6, 1–8.
Zhao, B., Gandhi, S., Yuan, C., Luo, Z., Li, R., Gårdsvoll, H., Sidenius, N., Huang, M., Ploug, M., 2015a. J. Mol. Biol. 427, 1389–1403.
Zhao, B., Gandhi, S., Yuan, C., Luo, Z., Li, R., Gårdsvoll, H., Sidenius, N., Huang, M., Ploug, M., 2015b. Data in Brief, vol. 5. pp. 107–113.